

Vibrational properties of phonons in random binary alloys: An augmented space recursive technique in the k -representation

Amitab Alam and Abhijit Mukherjee

S.N. Bose National Centre for Basic Sciences, JD Block, Sector III, Salt Lake City, Kolkata 700098, India

Abstract. We present here an augmented space recursive technique in the k -representation which include diagonal, off-diagonal and the environmental disorder explicitly: an analytic, translationally invariant, multiple scattering theory for phonons in random binary alloys. We apply the formalism to $Ni_{55}Pd_{45}$, $Ni_{38}Cr_{12}$ and $Ni_{50}Pt_{50}$ alloys which is not a random choice. Numerical results on spectral functions, dispersion curves and disordered induced FWHM's are presented. Finally the results are compared with the recent itinerant coherent potential approximation (ICPA) and also with experiments.

PACS numbers: 72.10.Dj

1. Introduction

Over the years, there have been many attempts to develop adequate approximations for properties of elementary excitations in disordered systems. Among these phonons are not only conceptually the simplest, but are also the most readily accessible to experimental verification. Neutron scattering experiments [1, 2, 3] have provided detailed information about lattice vibrations in random alloys. A satisfactory reliable theory is still lacking. The main reason for this is that, unlike the case of electrons in substitutionally disordered alloys, where the Hamiltonian can be expressed in a form where the disorder is diagonal in a real space representation x , the disorder in the dynamical matrix is essentially off-diagonal. To make things more complicated, the diagonal and off-diagonal disorders in the dynamical matrix are coupled by the force constant sum rule $\sum_{R \in R} \phi_{RR} = 0$, which ensures that no vibration can be excited in a uniform translation of the crystal as a whole. This sum rule imposes an environmental disorder on the force constants. That is, the disorder in the diagonal element of the dynamical matrix depends upon its near neighbours or its immediate environment. Hence a reliable theory for phonon excitations will be that which includes all the three kinds of disorders explicitly.

Corresponding author: email alam@bose.res.in

This is certainly true, for example, in a LMTO formalism in the absence of local lattice distortions

Let us look at the most successful mean field approximation : the single-site coherent potential approximation (CPA), introduced first by Taylor [4]. As the name itself suggests, it is a single site approximation and per se cannot deal adequately with off-diagonal disorder. Several authors have proposed schemes for generalizing the CPA and their approaches include geometrically scaled off-diagonal disorder [5, 6], linearly scaled off-diagonal disorder [7] and independent diagonal and off-diagonal disorder [7, 8, 9, 10]. Most of these schemes in practice lead to a single site CPA including off-diagonal disorder. These approaches suffer from two different kinds of drawbacks : first, there is no reason why the off-diagonal part of the dynamical matrix should scale either as the geometric mean or the arithmetic mean of the constituents. Secondly, often the extra assumptions lead to approximate Green functions which violate the essential herglotz analytic properties required to produce physically acceptable results. The augmented space approach suggested by Mookerjee [12] provided a very interesting starting point for the generation of appropriate approximations. The 2-site CPA proposed by Yussoufi and Mookerjee [11] for model systems and subsequently generalized by Mookerjee and Singh [13, 14] to realistic alloys was one successful approach. While it retained the herglotz properties of the approximate Green functions, the generalization of the 2CPA to larger clusters violated the lattice translational symmetry of the configurationally averaged Green function for homogeneous disorder. This was overcome subsequently by the traveling cluster approximation of Kaplan and Gray [8] also based on the augmented space method. Recently, Ghosh et al [16] have proposed a nearest neighbour traveling cluster CPA and have applied it to phonons in NiPt and NiPd alloys. In this communication we shall propose a different approximation procedure. We shall start from the augmented space method and use the recursion method of Haydock et al [19] to obtain the configurationally averaged Green functions. The termination of the continued fraction expansion will constitute the approximation. This will not only retain the herglotz analytic properties of the approximate averaged Green function, but also include the effect at a site of its neighbourhood, the size of which we can control. We shall incorporate the effect of the very distant environment by the use of accurate termination schemes proposed e.g. by Haydock [20], Luchini and Nex [21] or Beer and Pettifor [22]. Since we shall incorporate the lattice translation symmetry in the full augmented space (which is characteristic of homogeneous disorder) [23] within our approach, the drawback of the original cluster-CPAs used by Singh and Mookerjee [13, 14] will be overcome. Further, we shall use the local point group symmetries of the lattice and the configurations on it to drastically reduce the rank of the Hilbert space on which the recursion takes place (see Saha et al [15]). This will allow us to accurately account for large environments around a particular site. It is not immediately clear how easy it would be to extend the method proposed by Ghosh et al to larger sized clusters. The technique will be ideally suited for fast and accurate computation.

In Section 2, we shall introduce the basic formalism. In Sections 3 to 5 we shall present results for Ni₅₅Pd₄₅, Ni₈₈Cr₁₂ and Ni₅₀Pt₅₀ alloys and compare them with experiment. The choice of the systems is deliberate : NiPd has predominantly mass disorder, NiCr predominant disorder in the dynamical matrix ; NiPt has large disorder both in the mass and the dynamical matrix. Concluding remarks are presented in Section 6.

2. FORMALISM

2.1. The augmented space formalism for phonons

The basic problem in the theory of phonons is to solve a secular equation of the form

$$(M \omega^2 - D) u(R; \omega) = 0$$

where $u(R; \omega)$ is the Fourier transform of $u(R; t)$, the displacement of an atom from its equilibrium position R on the lattice, in the direction α at time t . M is the mass operator, diagonal in real space and D is the dynamical matrix operator whose tight-binding representation is of the form :

$$M = \sum_R \sum_{\alpha} m_R P_R \quad (1)$$

$$D = \sum_R \sum_{\alpha} \sum_{\beta} \sum_{R^0} X_{R\alpha} X_{R\beta} P_R + \sum_{R^0} T_{RR^0} \quad (2)$$

along with the sum rule

$$\sum_{R^0} T_{RR^0} = 0 \quad (3)$$

Here P_R is the projection operator $\sum_{\alpha} |R\rangle\langle R|_{\alpha}$ and T_{RR^0} is the transfer operator $\sum_{\alpha} |R\rangle\langle R^0|_{\alpha}$ in the Hilbert space H spanned by the tight-binding basis $|R\rangle$. R, R^0 specify the lattice sites and α, β the Cartesian directions. m_R is the mass of an atom occupying the position R and T_{RR^0} is the force constant tensor.

We shall be interested in calculating the displacement-displacement Green function in the frequency-wavevector space :

$$G(k; \omega^2) = \langle k | M \omega^2 - D^{-1} | k \rangle$$

where $|k\rangle$ is a state in the reciprocal space given by

$$|k\rangle = \frac{1}{N} \sum_R \exp(i k \cdot R) |R\rangle$$

Since the mass matrix M is perfectly diagonal, we can write

$$G(k; \omega^2) = \langle k | M^{-1/2} \omega^2 I - M^{-1/2} D M^{-1/2} | k \rangle \quad (4)$$

where

$$M^{-1/2} = \sum_R \sum_{\alpha} m_R^{-1/2} P_R$$

The equation (4) looks exactly like the Green function for the electronic case with $M^{-1/2} D M^{-1/2}$ playing the role of Hamiltonian H , ω^2 in place of energy and $M^{-1/2} |k\rangle$ is the starting state of recursion.

Let us now consider a binary alloy A_xB_y consisting of two kinds of atoms A and B of masses m_A and m_B randomly occupying each lattice sites. We wish to calculate the configuration-averaged Green function $G(k;w^2)$. We shall use the augmented space formalism (ASF) to do so. The ASF has been described in great detail earlier [24]. We shall indicate the main operational results and refer the reader to the above monograph for further details. The first operation is to represent the random parts of the secular equation in terms of a random set of local variables $f_{R\alpha}$ which are 1 if the site R is occupied by a A kind of atom and 0 if it is occupied by B. The probability densities of these variables may be written as :

$$Pr(n_R) = x \delta(n_R - 1) + y \delta(n_R) \\ = \int \delta(n_R - 1) = \int \delta(n_R - 1) \delta(n_R - N_R)^{-1} \delta(n_R - 1) \delta(n_R - 1)$$

where x and y are the concentrations of the constituents A and B with $x + y = 1$. N_R is an operator defined on the configuration space Ω_R of the variable n_R . This is of rank 2 and is spanned by the states $f_{R\alpha}$; $j_{R\alpha}$:

$$N_R = x P_R + y P_R + P \frac{1}{xy} (\delta_{R\alpha} + \delta_{R\beta})$$

The augmented space theorem [12] now states that the configuration average of the Green function $G(k;w^2)$ may be written as

$$G(k;w^2) = \int G(k;w^2; f_{R\alpha}) Pr(n_R) dn_R \\ = \int h_{k\alpha} f_{R\alpha} \int w^2 P \int M^{-1} \int M^{-1} \int M^{-1} \int M^{-1} \int k_{\alpha} f_{R\alpha} (5)$$

where M^{-1} and \mathcal{D} are the operators which are constructed out of M^{-1} and D by replacing all the random variables n_R (or $n_{R\alpha}$) by the corresponding operators N_R (or $N_{R\alpha}$). These are the operators in the augmented space $\Omega = H$. The configuration space $\Omega = \Omega_R$ is of rank 2^N for a system of N-lattice sites with binary distribution. A basis in this space is denoted by the cardinality sequence $f_{R\alpha} = f_{R_1}; f_{R_2}; \dots; f_{R_N}$ which gives us the positions where we have a $j_{R\alpha}$ configuration. The configuration $f_{R\alpha}$ refers to a null cardinality sequence i.e. one in which we have $j_{R\alpha}$ at all sites.

Let us now carry out the ASF operations in some detail. The mass m_R for site R can then be expressed as

$$m_R^{-1} = m_A^{-1} n_R + m_B^{-1} (1 - n_R) \\ = m_B^{-1} + (m_A^{-1} - m_B^{-1}) n_R$$

where

$$(m_A^{-1} - m_B^{-1}) = m_A^{-1} - m_B^{-1}$$

Therefore

$$M^{-1} = \sum_R h_{k\alpha} m_B^{-1} + n_R (m_A^{-1} - m_B^{-1}) P_R (6)$$

In augmented space formalism,

$$\begin{aligned} n_R \cdot N_R &= x p_R'' + y p_R^\# + p \overline{xy} (p_R^\# + p_R'') \\ &= x \Gamma + (y - x) p_R^\# + p \overline{xy} T_R'' \end{aligned}$$

Using the above we get,

$$\overline{M}^{-1=2} = m_1^{-1=2} \Gamma + m_2^{-1=2} \sum_R p_R^\# + m_3^{-1=2} \sum_R T_R'' + E_R$$

where

$$\begin{aligned} m_1^{-1=2} &= x m_A^{-1=2} + y m_B^{-1=2} \geq 0 \\ m_2^{-1=2} &= (y - x) (m)^{-1=2} > 0 \\ m_3^{-1=2} &= p \overline{xy} (m)^{-1=2} > 0 \end{aligned}$$

(7)

Similarly the random off-diagonal force constants m_{RR^0} between the sites R and R^0 can be written as :

$$\begin{aligned} m_{RR^0} &= m_{AA} n_R n_{R^0} + m_{BB} (1 - n_R)(1 - n_{R^0}) + m_{AB} [n_R (1 - n_{R^0}) + n_{R^0} (1 - n_R)] \\ &= m_{BB} + (m_{AA} + m_{BB} - 2 m_{AB}) n_R n_{R^0} + (m_{AB} - m_{BB}) (n_R + n_{R^0}) \end{aligned}$$

(8)

Let us define the following :

$$\begin{aligned} (1) &= x m_{AA} - y m_{BB} + (y - x) m_{AB} \\ (2) &= m_{AA} + m_{BB} - 2 m_{AB} \end{aligned}$$

In augmented space the off-diagonal force constant matrix becomes an operator :

$$\begin{aligned} e_{RR^0} &= \sum_{RR^0} m_{RR^0} \Gamma + \sum_{RR^0} (1) (y - x) (p_R^\# + p_{R^0}^\#) + p \overline{xy} (T_R'' + T_{R^0}'') + \dots \\ &+ \sum_{RR^0} (2) (y - x)^2 p_R^\# p_{R^0}^\# + p \overline{xy} (y - x) p_R^\# T_{R^0}'' + p_{R^0}^\# T_R'' + xy T_R'' T_{R^0}'' + \dots \\ &= \sum_{RR^0} m_{RR^0} T_{RR^0} \end{aligned}$$

(9)

This equation is now exactly in the form in which recursion method may be applied. At this point we note that the above expression for the averaged $G(k; \omega)$ is exact. The recursion transforms the basis through a three term recurrence relation as

$$\begin{aligned} j_{1i} &= j_i \quad ; \quad j_{0i} = 0 \\ j_{n+1i} &= \mathcal{D}_{\text{eff}} j_{ni} - a_n j_{n-1i} + b_n^2 j_{n-2i} \end{aligned} \quad (13)$$

The averaged Green's function can then be written as a continued fraction

$$G(k; \omega) = \frac{b_1^2}{\omega - a_1(k) - \frac{b_2^2(k)}{\omega - a_2(k) - \frac{b_3^2(k)}{\ddots}}}$$

where,

$$a_n(k) = \frac{h_n \mathcal{D}_{\text{eff}} j_{ni}}{h_n j_{ni}} \quad \text{and} \quad b_n^2(k) = \frac{h_n j_{ni}}{h_{n-1} j_{n-1i}} \quad ; \quad b_1^2 = 1$$

So far the expression for the averaged Green function is exact. Approximations are introduced at this stage for its actual numerical evaluation. The mean-field theories essentially obtain the self-energies because of disorder scattering, self-consistently and approximately and then calculate the averaged Green function either from the Green function without disorder or the virtual crystal Green function. The Coherent potential approximation (CPA) proposed by Soven [25], the cluster CPA proposed by Mookerjee and Singh [13, 14], the traveling cluster approximation (TCA) proposed by Mills and Ratanavaraksa [9] and Kaplan et al [10] and the itinerant CPA (ICPA) proposed by Ghosh et al [16] basically all belong to this category. The latest work referenced represent the most sophisticated version of the mean-field theories. We shall propose an approximation that will start from the infinite continued fraction and approximate its asymptotic part by an analytic termination procedure. The coefficients a_n, b_n are calculated exactly up to a finite number of steps and the asymptotic part is then replaced by a terminator. Haydock and co-workers [20] have carried out extensive studies of the errors involved and precise estimates are available in the literature. Several terminators are available and we have chosen to use that of Luchini and Nex [21]. If we calculate the coefficients up to the n -th step exactly the first $2n$ moments of the density of states are reproduced exactly. The terminator ensures that the approximate Green function has herglotz analytic properties which also tells us that the approximate density of states is always positive definite and the spectrum is always real. The terminator is also so chosen that the asymptotic moments are also accurately reproduced. This is a generalization of the method of moments, with the additional restriction that the asymptotically large moments are also accurately obtained.

In the absence of disorder in the problem, the Green function for a given mode is of the form :

$$G_0(k; \omega) = \frac{1}{\omega^2 - \omega_0^2(k)}$$

The spectral function $A_0(k; \omega)$ is a delta function of the form $\delta(\omega - \omega_0^2(k))$. If we write :

$$\begin{aligned} \omega(k; \omega^2) &= \omega_1(k) \omega_0^2(k) + \frac{b_2^2(k)}{\omega^2 - \omega_2^2(k)} \\ &\quad \dots \\ &= \omega_1(k) \omega_0^2(k) + \omega(k; \omega^2) \end{aligned} \tag{14}$$

Then,

$$G(k; \omega^2) = G_0(k; \omega^2) \omega(k; \omega^2)$$

Obviously from above $\omega(k; \omega^2)$ is the disorder induced selfenergy. Damped vibrations occur with reduced frequencies at $\omega_0^2(k)$ which are the solutions of the implicit equation :

$$\omega_0^2(k) - \omega_1(k) - \omega(k; \omega_0^2(k)) = 0$$

and their disorder induced widths are :

$$W(k; \omega_0^2(k)) = \frac{1}{\omega} = \omega(k; \omega_0^2(k)) \tag{15}$$

The average spectral function $A(k; \omega^2)$ for a mode labelled i is related to the averaged Green function in reciprocal space as

$$A(k; \omega^2) = \frac{1}{\omega} \lim_{\sigma \rightarrow 0} \text{Im} \sum_{i=1}^n G(k; \omega^2 - i\sigma) \tag{16}$$

The averaged density of states is given by :

$$n(\omega) = \frac{2\omega}{3} \int_{BZ} \frac{d^3k}{8\pi^3} A(k; \omega^2)$$

Here i labels the particular normal mode branch and BZ is the Brillouin zone.

The dispersion curves for different modes are then obtained by numerically calculating the peak frequencies of the spectral function. This averaged spectral function gives, in principle, a proper description of the dynamics but it does not involve any weighting by scattering lengths. The dispersion curves so obtained are nearly the same as those obtained experimentally from the peak frequencies of the coherent structure factors S_{coh} . This is because the coherent structure factors are nothing but the averaged Green functions weighted by the coherent scattering lengths.

| | Ni | Pd | Pt | Cr |
|---|---------------------------------|------------------|---------------------------------|---------------------------------|
| 1. Atomic number | 28 | 46 | 78 | 24 |
| 2. Atomic mass (amu) | 58.71 | 106.4 | 195.09 | 51.996 |
| 3. Free atom valence confg | 3d ⁸ 4s ² | 4d ¹⁰ | 5d ⁹ 6s ¹ | 3d ⁵ 4s ¹ |
| 4. Lattice constant (fcc) | 3.524 | 3.8904 | 3.924 | 3.68 (fcc) 2.89 (bcc) |
| 5. Elastic constants at 296°K (10 ¹² dyne/cm) | | | | |
| C ₁₁ | 2.461 | 2.270 | 3.467 | 3.5 |
| C ₁₂ | 1.501 | 1.759 | 2.507 | 0.678 |
| C ₄₄ | 1.220 | 0.717 | 0.765 | 1.010 |
| 6. n-n force constants (in units of dyne/cm) | | | | |
| 1XX | 17319 | 19337 | 26358 | 37483 |
| 1XY | 19100 | 22423 | 30317 | 17453 |
| 1ZZ | -436 | -2832 | -7040 | -13229 |

Table 1. General properties of fcc Ni, Pd, Pt and Cr. The force constants for Ni, Pd and Pt are taken from [26] and that for Cr is taken from [14]

The intensities and the line shapes measured from S_{coh} and the imaginary part of Green function may differ significantly, but the peak positions will generally differ little.

The disorder induced widths are more sensitive to effects of randomness as compared to the frequencies (i.e. dispersion curves), and as such will be one of the focus of this work. In order to extract the full width at half maxima (FWHM), we have fitted the spectral functions to Lorentzians exactly as the experimentalists do to extract the same. In the following three Sections, we present our calculations on Ni₅₅Pd₄₅, Ni₈₈Cr₁₂ and Ni₅₀Pt₅₀ alloys. The choice is not arbitrary. Mass disorder dominates in NiPd alloys while force constant disorder is large in NiCr alloys. NiPt alloys have large disorder both in mass and force constants. Since in the phonon problem we have both kinds of disorder, it would be interesting to note the interplay between them in this series of alloys. The concentrations are chosen so that we may compare our results with existing work.

We have chosen a nearest neighbour force constant model, with dynamical matrices fitted to reproduce the dispersion curves for the constituent elements. Such a model is rather crude, and certainly much better models exist in literature. Our aim in this communication is to propose the augmented space recursion as a useful technique to study effects of diagonal, off-diagonal and environmental disorder. A accurate model building or obtaining the force constants from first-principles total energy calculations will be postponed for future work.

3. Results and Discussion

3.1. The Ni₅₅Pd₄₅ Alloy

A look at Table 1 immediately shows us that for NiPd alloys, the dominant disorder is in the mass. Force constants in Pd are only about 15% larger than those in Ni. We shall choose the Ni₅₅Pd₄₅ alloy for the application of our formalism developed in section 2. This particular alloy has already been studied within the ICPA by Ghosh et al [16], CCPA by Mookerjee and Singh [14] and experimentally [1] by inelastic neutron scattering. The alloy forms a continuous series of face centered cubic solid solutions of all concentrations and there are no indications of long range order down to 0°C.

In Figure 1 we display the total spectral functions obtained from our recursion calculation along the highest symmetry directions ($[100]$, $[110]$, $[111]$), ω_{max} for different branches. For a particular direction and branch the different curves indicates the spectral functions for various q points starting from the lowest value (i.e. $q = 0$) to the edge of the Brillouin zone (i.e. $q = 1$ in units of $2\pi/a$). The first thing to note is that the spectral functions are (in contrast to Lorentzian shape) often asymmetric near the resonances. The asymmetries can be described as a tendency of more scattering to occur near the resonance frequencies. In other words the shape of a mode with a frequency slightly lower or higher than that of a resonance tends to have a second peak or wide tail over the resonance region. In fact if one looks at the $[100]$ L or T1 (doubly degenerate) and $[111]$ L or T1 or T2 (3-fold degenerate) branches, the shape of a doubly peaked spectral function is much more clear. Out of these two peaks, one peak corresponds to the dispersion curve for the longitudinal mode (L) and the other peak to the transverse mode (T). Experimentally, for some neutron groups corresponding to transverse phonons with frequencies just below the lower resonance, definite asymmetry to the right was observed. Such asymmetries are clearly observed for the $[100]$ T and $[111]$ T branches. It is important to note that the spectral functions have a pronounced q and branch dependence.

In Figure 2 we display the dispersion curves, which were constructed by numerically determining the peaks in the spectral functions. In this communication our main focus is the development of the augmented space recursion method. A accurate determination of the force constants shall be left for the future. Ghosh et al [16] have attempted a much more detailed determination of the force constants. We have also tried out their parameters, and do not get anything qualitatively new. We keep κ_{NiNi} and κ_{PdPd} the same as those of pure materials and assume that $\kappa_{NiPd} = 0.5(\kappa_{NiNi} + \kappa_{PdPd})$. These dispersion curves (solid lines) are compared with the experimental results [1] (filled circles). The dotted lines span the calculated FWHM's. The procedure of calculating FWHM's has already been discussed. The asymmetry in the widths is again clearly observed in the two transverse branches quoted above. The results are in good agreement with the experiment for all the three symmetry directions and for each branch. Agreement can be achieved by varying only one parameter in the force constant matrix. This suggests that the force constant disorder is weak and the system is dominated by the mass disorder, as is clear from the numerical values of the parameters given in Table 1. If one looks at the previous results for the dispersion curves (i.e. VCA, CPA and ICPA curves) [16], it will be clear that in the low wave vector regime, there is no distinction between these results

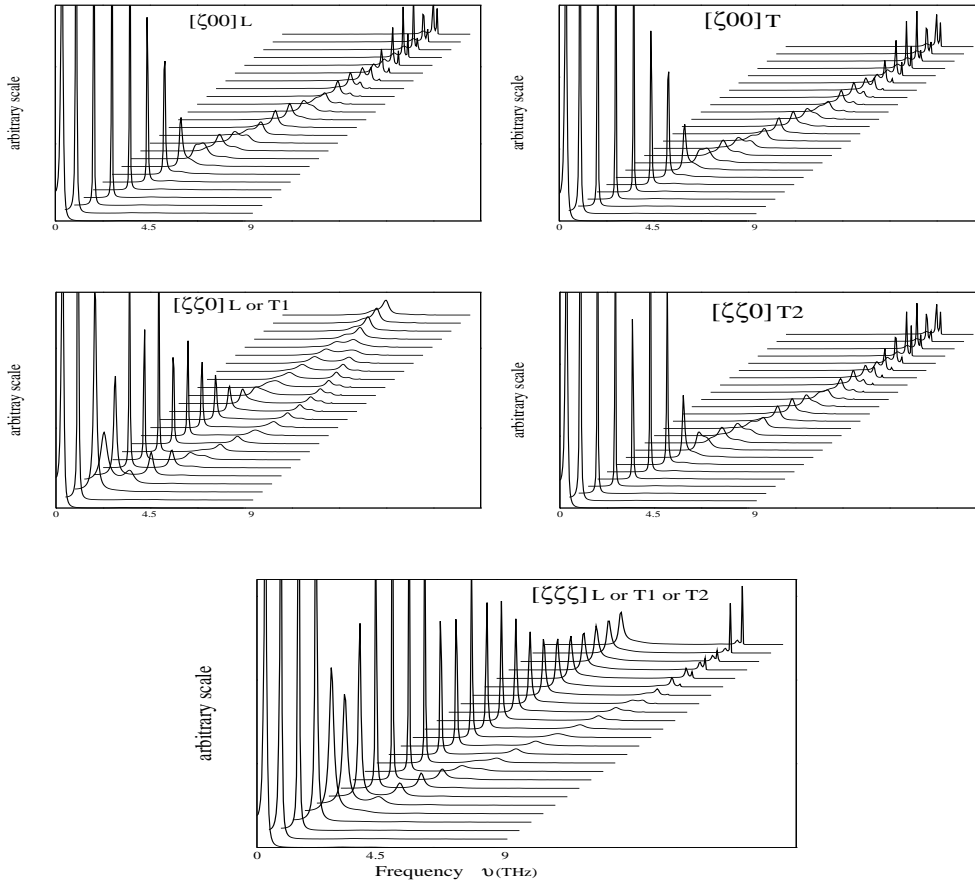


Figure 1. Total spectral functions in different directions with different branches for Ni_5Pd_{45} . In each of the different directions and branches, the various curves indicate the total spectral functions for various ν values starting from the lowest value to the edge of the Brillouin zone. In $[00]$ direction T1 and T2 modes are degenerate, in $[\zeta 0]$ direction L and T1 modes are degenerate and in $[\zeta\zeta]$ direction all the three modes are degenerate. The y-axis is in an arbitrary scale with heights scaled to the maximum height. Different curves for different ν values are shifted along the x-axis in order to facilitate vision.

and ours, Because the self averaging of both mass and force constants over a single wavelength reduces the CPA, ICPA and the ASR results to become close to the VCA. However as we move toward high wave vectors, the VCA curve deviates from the experimentally observed one and lies lower in frequency as compared to the ICPA and the ASR results. The reason is that VCA uses an averaged mass. In contrast to this, for those theories which capture the effect of mass fluctuation (as do the ICPA and the ASR), the lighter atoms (Ni in this case) dominate in the high wave vector region and push the frequencies up. That is why our results agree very well across the Brillouin zone.

The FWHM's are much more sensitive to approximations as compared to the

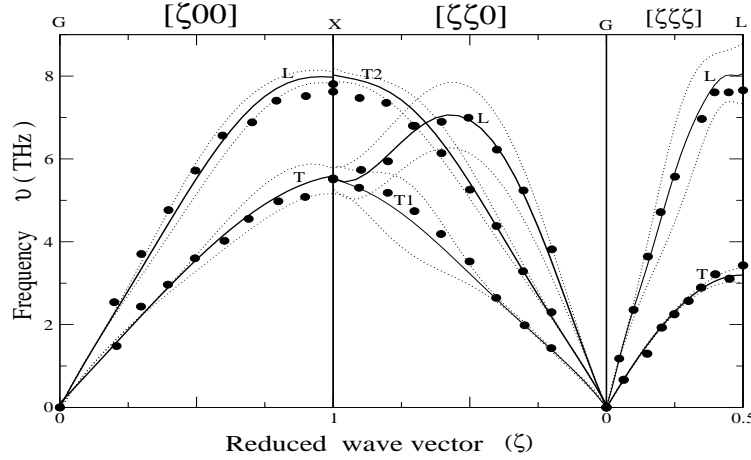


Figure 2. Dispersion Curves (frequency vs. reduced wave vector) for $Ni_{5}Pd_{45}$ calculated from recursion (solid line). The force constants used are given in the text. The filled circles are the experimental data [1]. In all the three panels the thin dotted lines span the FWHM's.

frequencies. These are shown in figure 3. Our results show very strong branch and wave-vector dependent widths and in good agreement with the experimental results of Kamitakahara and Brockhouse. The single site CPA yields branch and k independent widths. It cannot capture the essentially off-diagonal disorder of the problem. The ICPA and the ASR manages to capture this feature. One should note that the spectral functions are often asymmetric in shape and the usual Lorentzian fits carried out by most people may not be valid.

3.2. The $Ni_{88}Cr_{12}$ alloy

We shall choose this alloy as being the nearest to that studied experimentally by Bosi et al [27]. Determination of the force constant matrices for this alloy becomes difficult, because pure Cr is body centered cubic, but alloyed with Ni, up to 30% Cr it forms face centered cubic alloys. The force constants of pure Cr may be nothing like those of Cr in this alloy. Until we are able to determine these from a more first-principles type approach, our determination of the force-constants for this alloy will remain tentative. We shall consider a hypothetical fcc Cr, whose force constants are related to the elastic constants of bcc Cr via :

$$\begin{aligned}
 C_{11} + C_{12} &= 4(f_1 + f_0 + f_t) = a \\
 C_{11} - C_{12} &= (f_1 + 5f_0 + f_t) = a \\
 C_{44} &= (f_1 + f_0 + 2f_t) = a
 \end{aligned}$$

The values of C_{11} , C_{12} and C_{44} are taken from Leibfried and Breuer [28] (given in Table 1). In figure 4 we display the spectral functions for $Ni_{88}Cr_{12}$ along the

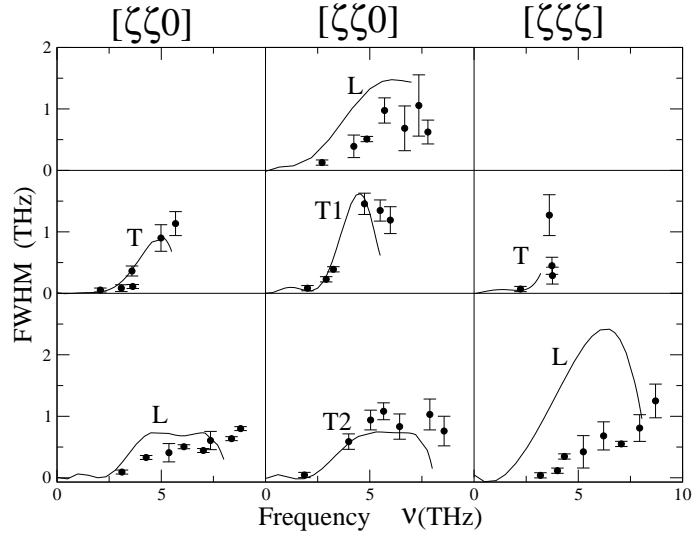


Figure 3. Full widths at half maximum for the NiPd alloy as function of frequency for different directions in k-space and different modes. The filled circles along with the error bars are the experimental data [1]

highest symmetry directions for different ζ -values. There is strong evidence of branch dependent widths as also asymmetry in certain directions. This lends credence to our belief that force-constant disorder leads to both asymmetry and strong wave-vector and frequency dependence of the line-shapes.

The influence of force constant disorder may be demonstrated more prominently in the dispersion curves and widths. In figure 5, we display the dispersion curves along with the FWHM's using the force constants of Table 1. The procedure has already been discussed in the previous section. These dispersion curves compare well with the experimental results [27] as well as the 2 CPA results of Mookerjee and Singh ([14]) (filled circles). The dotted lines span the calculate FWHM's. It should be noted that in the low frequency region, the widths are small but start to become significant as the phonon frequency increases. The widths are comparatively larger in the $[00]L$, $[\zeta\zeta]L$ and $[\zeta 0]T2$ branches for high ζ -values. Looking at the dispersion curves, one should notice that the behaviour of the natural widths were somehow complemented in the behaviour of the frequencies. There is little evidence of resonances. This is expected, since clear cut resonances are characteristics of large mass disorders only.

In figure 6 we show the FWHM as a function of frequency. It is clear that there is strong evidence of mode and k-dependence. The FWHM's are very large and asymmetric for the longitudinal modes near the band edge frequencies.

It is obvious from the above discussions that the force constant disorder plays a significant role in Ni_8C_{12} ; and a theory capturing only mass disorder effect (e.g. like CPA) fails to provide various essential features.

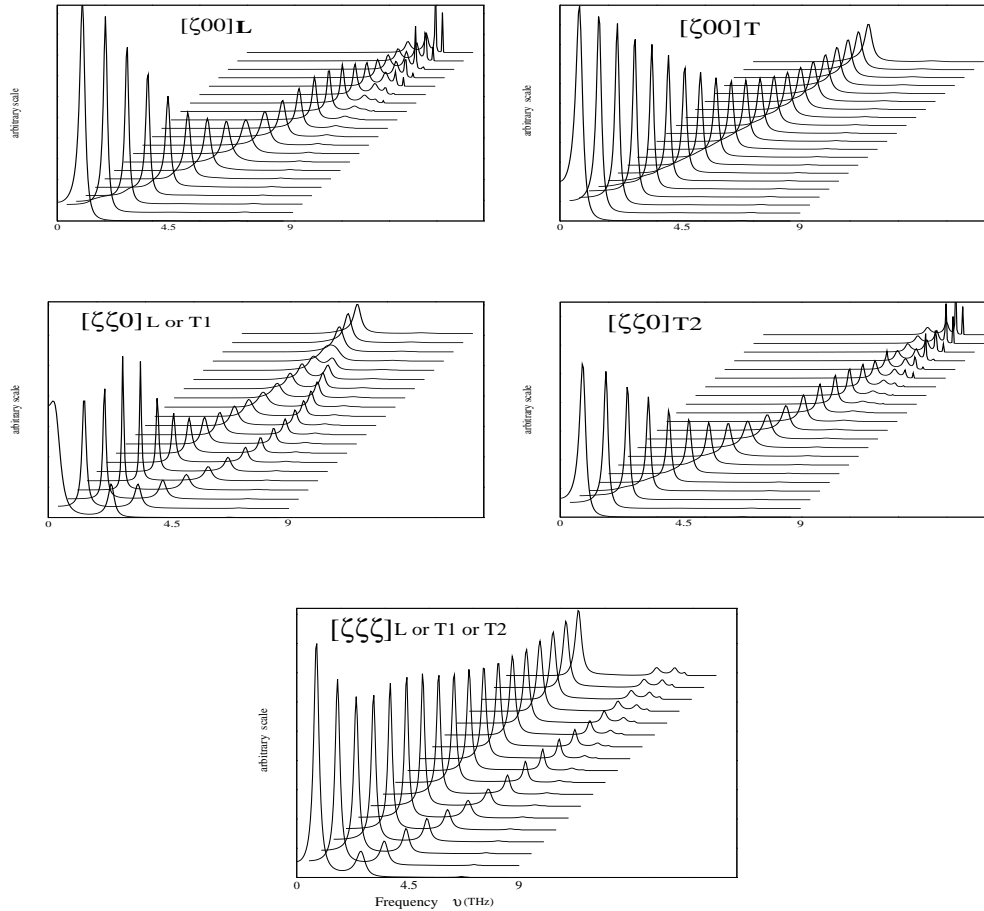


Figure 4. Total spectral functions in different directions with different branches for $\text{Ni}_8\text{Cr}_{12}$. In each of the different directions and branches, the various curves indicate the total spectral functions for various α values starting from the lowest value to the edge of the Brillouin zone. In $[000]$ direction T1 and T2 modes are degenerate, in $[100]$ direction L and T1 modes are degenerate and in $[111]$ direction all the three modes are degenerate. The details are given in the text.

3.3. The $\text{Ni}_{50}\text{Pt}_{50}$ alloy

Being encouraged by the right trend of theoretical results toward the experimental results in the $\text{Ni}_{55}\text{Pd}_{45}$ and $\text{Ni}_{88}\text{Cr}_{12}$ alloys, where either of the two disorders { diagonal and off-diagonal dominates, we now apply our formulation to NiPt alloys where both disorders are predominant. The mass ratio $m_{\text{Pt}}/m_{\text{Ni}}$ is 3.3 (quite large compared to previous alloys) and the nearest neighbour force constants of Pt are on an average 55% larger than those in Ni. Tsunoda et al [2] have studied this system thoroughly covering a wide range of concentration ($x=0.05, x=0.3, x=0.5$) by inelastic neutron scattering. In our case, we have considered $x=0.5$ where we expect the disorder induced scattering to have the strongest effect.

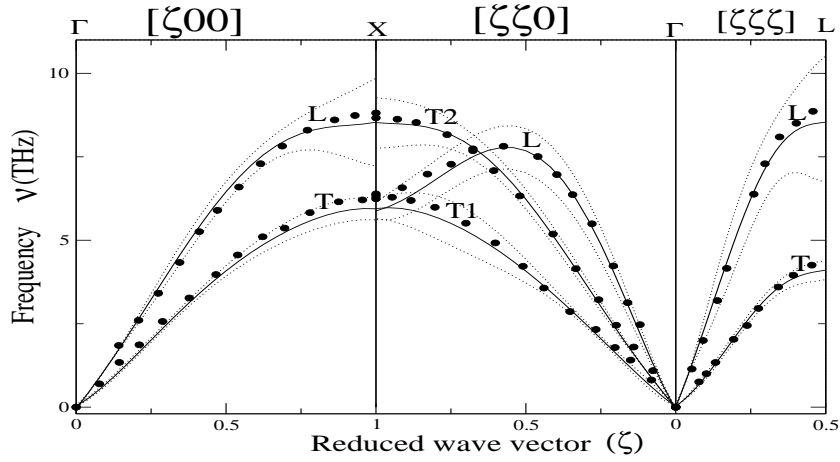


Figure 5. Dispersion Curves (frequency vs. reduced wave vector) for $NiCr$ alloy calculated from recursion (solid line). The force constants used are given in the text. The filled circles are the 2 CPA results [14]. In all the three panels the thin dotted lines span the FWHM's.

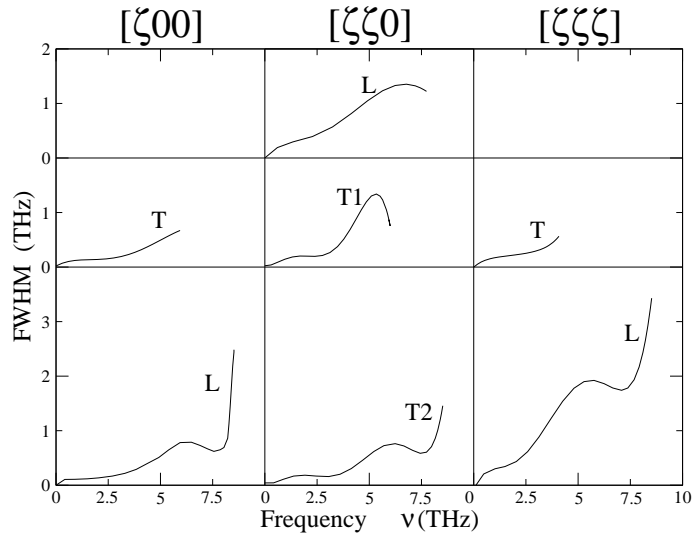


Figure 6. Full widths at half maximum for the $NiCr$ alloy as function of frequency for different directions in k -space and different modes.

In Fig 7, we display the total spectral functions along the highest symmetry directions for different modes. For a particular direction and branch, the various curves indicate the spectral functions for various α -values; starting from the lowest ($\alpha = 0$) to the highest value ($\alpha = 1$, in units of $2/a$). In this case, the spectral functions show few extra features: Even in $[00]L$, $[00]T$ and $[00]T_2$ modes, unlike the

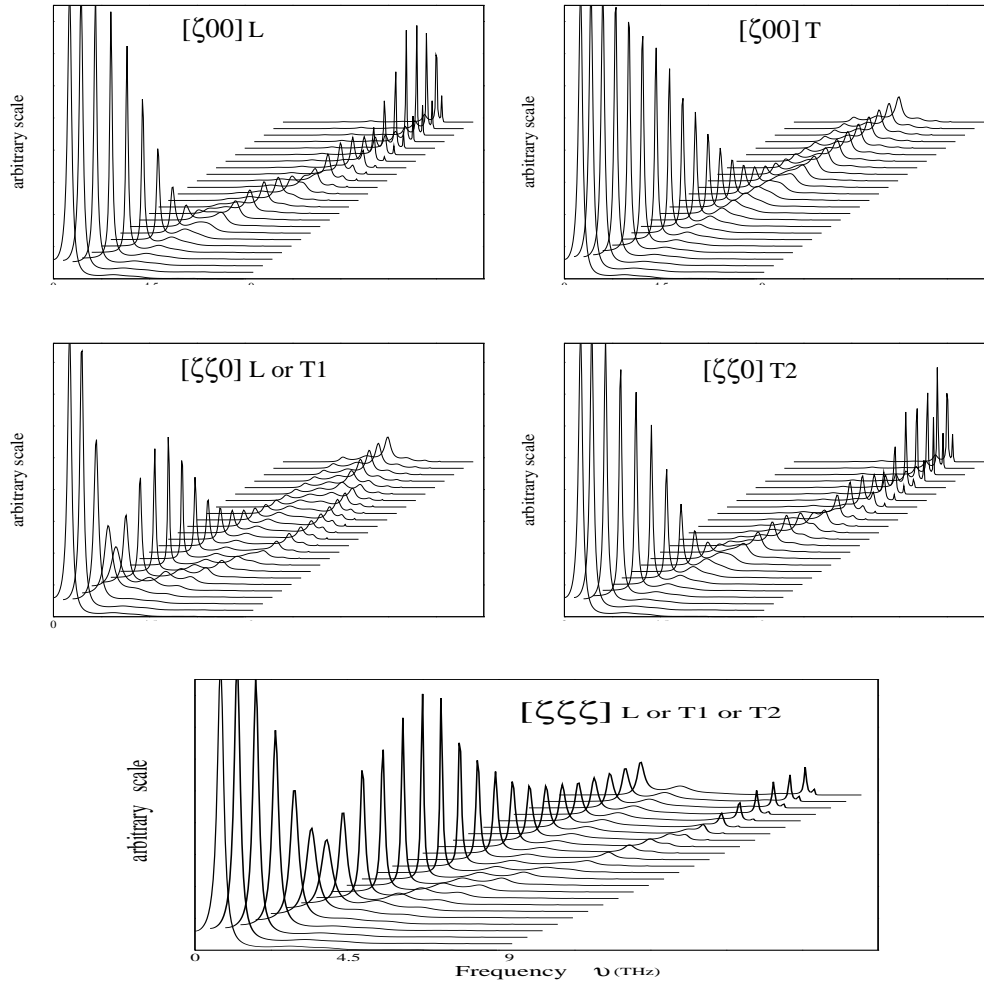


Figure 7. Total spectral functions in different directions with different branches for $\text{Ni}_{50}\text{Pt}_{50}$. In each of the different directions and branches, the various curves indicate the total spectral functions for various α values starting from the lowest value to the edge of the Brillouin zone. In $[100]$ direction T1 and T2 modes are degenerate, in $[110]$ direction L and T1 modes are degenerate and in $[111]$ direction all the three modes are degenerate. The details are given in the text.

In the previous two cases the spectral functions have one usual well defined peak (observed more clearly in the middle regime of the Brillouin zone) along with a weakly defined peak with no gap in between. The occurrence of such a weakly defined peak is due to the inclusion of force constant disorder. Ghosh et al ([16]) have argued that it is entirely because of the off-diagonal disorder in the force constants. We refer the reader to their paper for the detailed arguments. Here we note that the feature is equally well reproduced in our augmented space recursive technique as well, why this should be so.

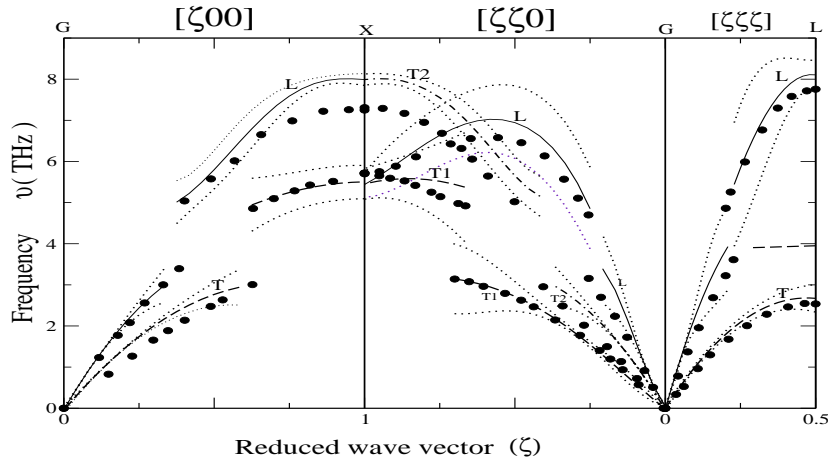


Figure 8. Dispersion Curves (frequency vs. reduced wave vector) for $Ni_{50}Pt_{50}$ calculated from recursion . The force constants used are given in the text. The solid lines are the L-branch in all the three panels, the dashed lines are the T-branch in the left and right panels. In the $[\quad 0]$ direction the dashed line indicate the T1 branch while the dot-dashed line indicate the T2 branch. The filled circles are the IC-PA results [16]. In all the three panels the thin dotted lines span the FWHM's.

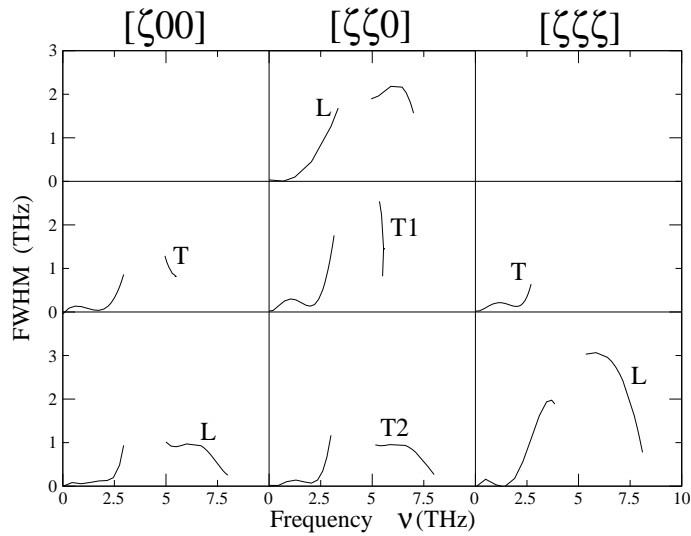


Figure 9. Full widths at half maximum for the $Ni_{50}Pt_{50}$ alloy as function of frequency for different directions in k-space and different modes.

The effect of force constant disorder can be understood more clearly by looking at the dispersion curves and widths.

In figures 8 and 9 we display the dispersion curves and widths obtained in the recursion using the force constants as given in the text. These dispersion curves (solid lines) are compared with that calculated in the ICPA (filled circles) by Ghosh et al [16]. The mismatch at the band edges along the $[100]$ and $[110]$ directions are due to the different inputs for the force constants in the two works. The aim of this work was to establish the ASR as a computationally fast and accurate method for phonon calculations for random alloys. Our ultimate goal is to obtain the force constants from first principles calculations, rather than parameter fitting. We have checked that use of the parameters of Ghosh et al ([16]) yields almost identical results across the Brillouin zone.

For all the three panels the thin dotted lines indicate the FWHM's. Unlike the previous two cases, the dispersion curves in this case have very different characteristic features. The splitting of the curves in all the three symmetry directions is the main feature. This is due to strong resonances, a feature of large mass disorder. Also as one can see that near the resonances (around 4 THz) the FWHM becomes very large. Tsunoda finds this resonance near 3.8 THz, while the CPA gives a rather lower value of 3 THz. If we look at the spectral functions shown in figure 7 we note that around 7 THz there is a third small peak split from the main branch. This evidence of a weak resonance was also speculated by Mookerjee and Singh ([13]). The overall agreement of our dispersion curves with those calculated in the ICPA is good except in the high wave vector region. The deviation becomes larger as we move from the middle of the zone toward the zone-edge. As discussed, this is because of the different inputs given in the two calculations. In ICPA, the authors have used $\gamma_{NiPt} = 0.8 \gamma_{NiNi}$ for all γ , however in our case $\gamma_{NiPt} = \frac{1}{2}(\gamma_{NiNi} + \gamma_{PtPt})$, which is greater than that taken in the ICPA. That is why we get slightly larger frequency band widths as compared to the ICPA ones.

In figure 10 we plot the density of states vs. frequency (THz) for NiPd and NiPt using the real space augmented space recursion ([29]). The results agree well with the earlier 2CPA work of Mookerjee and Singh ([13, 14]). However, the density of states as such is not very sensitive to different mean-field approximations, and we show these results for the sake of completeness.

4. Discussion and conclusions

We have set up the augmented space recursion in reciprocal space for the study of phonon dispersion and disorder induced line-widths and line-shapes for random binary alloys. The technique takes into account both diagonal disorder in the masses, the off-diagonal disorder in the force constants and the environmental disorder in the diagonal term of the force constants arising out of the sum rule. The approximation involving termination of continued fraction expansions of the Green function retains the essential herglotz analytic properties. We have applied the method to three classes of alloys: NiPd where mass disorder dominates, NiCr where force constant disorder dominates and NiPt where both dominate. Wherever possible we have compared our results with neutron scattering data as well as the most sophisticated mean-field theory recently proposed by Ghosh et al ([16]). Both qualitatively and quantitatively our results agree well with the available data. We propose the technique as a computationally efficient method for the study of phonons in disordered systems. Our approach here

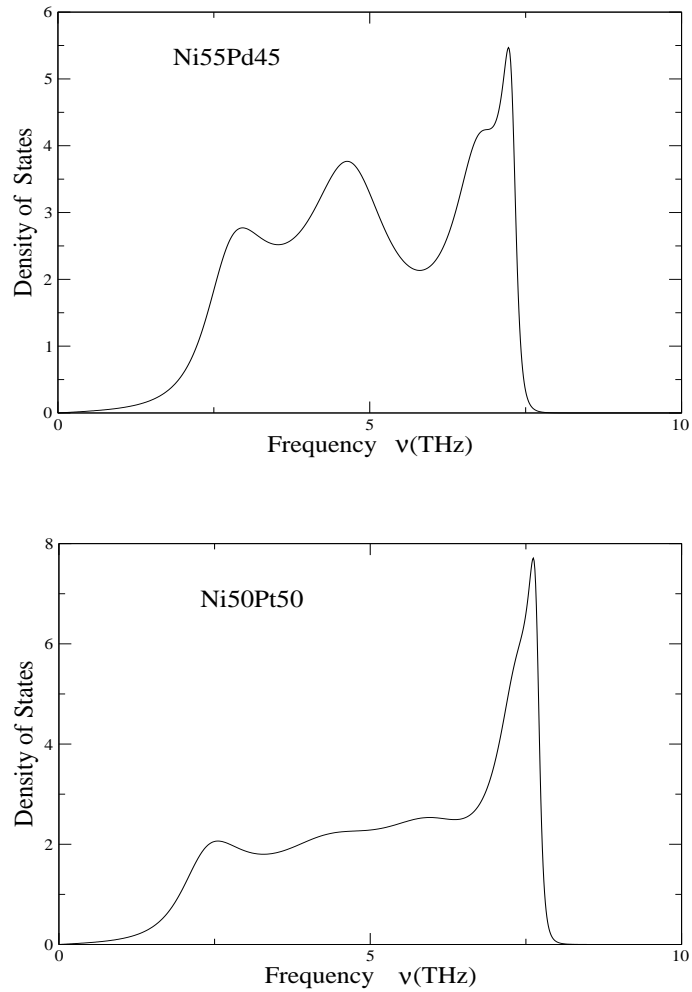


Figure 10. DOS/THz-atom vs. frequency for (top) NiPd and (bottom) NiPt calculated using the standard real space ASR

made no attempt to obtain the force constant themselves from first principles, but rather resorted, as others did earlier, to fitting them from experimental data on the constituent metals. Our future endeavor would be to rectify this, and attempt to obtain the dynamical matrix itself from more microscopic theories.

Acknowledgments

A.A. would like to thank the Council of Scientific and Industrial Research, India, for financial assistance.

References

- [1] W. A. Kamitakahara and B. N. Brockhouse, *Phys. Rev. B* **10**, 1200 (1974).
- [2] Y. T. Sunoda, N. Kunitomi, N. Wakabayashi, R. M. Nicklow and H. G. Smith, *Phys. Rev. B* **19**, 2876 (1979).
- [3] R. M. Nicklow in *Methods of Experimental Physics* (Academic Press, 1983), Vol. 23, p. 172.
- [4] D. W. Taylor, *Phys. Rev.* **156**, 1017 (1967).
- [5] H. Shiba, *Prog. Theor. Phys.* **40**, 942 (1968).
- [6] G. Grunewald, *J. Phys. F: Met. Phys.* **6**, 999 (1976).
- [7] T. Kaplan and M. M. Ostoller, *Phys. Rev. B* **9**, 353 (1974).
- [8] T. Kaplan and L. J. Gray, *Phys. Rev. B* **14**, 3462 (1976); *Phys. Rev. B* **24**, 1872 (1981).
- [9] R. Mills and R. Ratanavaraksa, *Phys. Rev. B* **18**, 5291 (1978).
- [10] T. Kaplan, P. L. Leath, Gray L. J. and D. Iehl H. W., *Phys. Rev. B* **10**, 1200 (1980).
- [11] M. Yussouf and A. Mookerjee, *J. Phys. C: Solid State Phys.* **17**, 1009 (1984).
- [12] A. Mookerjee, *J. Phys. C: Solid State Phys.* **6**, L205 (1973).
- [13] A. Mookerjee and R. P. Singh, *J. Phys. C: Solid State Phys.* **18**, 4261 (1985).
- [14] A. Mookerjee and R. P. Singh, *J. Phys. F: Met. Phys.* **18**, 2171 (1988).
- [15] I. Dasgupta, T. Saha and A. Mookerjee, *J. Phys.: Condens. Matter* **8**, 1979 (1996).
- [16] S. Ghosh, P. L. Leath, and Morrel H. Cohen *Phys. Rev. B* **66**, 214206 (2002).
- [17] R. Haydock, V. Heine and M. J. Kelly, *J. Phys. C: Solid State Phys.* **5**, 2845 (1975).
- [18] T. Saha, I. Dasgupta and A. Mookerjee, *J. Phys.: Condens. Matter* **6**, L245 (1994).
- [19] R. Haydock, V. Heine and M. J. Kelly, *J. Phys. C: Solid State Phys.* **5**, 2845 (1972).
- [20] R. Haydock, *Solid State Phys.* (Academic Press, New York) **35**, 216 (1980).
- [21] M. U. Luchini and C. M. M. Nex, *J. Phys. C: Solid State Phys.* **20**, 3125 (1987).
- [22] N. Beer and D. G. Pettifor, *Electronic Structure of Complex Systems* ed. P. Phariseau and W. M. Temmerman (Plenum, New York, 1984) p. 769.
- [23] S. Ghosh, N. Das and A. Mookerjee, *J. Phys.: Condens. Matter* **9**, 10701 (1997).
- [24] A. Mookerjee, *Electronic Structure of Alloys, Surfaces and Clusters* (ed. D. D. Sama and A. Mookerjee) (Taylor Francis, London) (2003).
- [25] P. Soven, *Phys. Rev.* **156**, 809 (1967).
- [26] D. H. Dutton, B. N. Brockhouse and A. P. Miller, *Can. J. Phys.* **50**, 2915 (1972).
- [27] P. Bosi, F. Dupre, F. Menzinger, F. Sacchetti and M. C. Spinelli, *Nuovo Cim. Lett.* **21**, 436 (1978a); *Nuovo Cim.* **46**, 337 (1978b).
- [28] G. Leibfried and N. Breuer, *Point Defects in Metals I* (Springer Tracts in Modern Physics, Vol. 81, Springer Verlag Berlin, New York).
- [29] A. Mookerjee, *J. Phys. C: Solid State Phys.* **6**, 1340 (1973).